Aqueous solution-gel precursors for LiFePO4 lithium ion battery cathodes, their decomposition and phase formation

DOI: 10.1007/s10971-017-4467-z
Handle: http://hdl.handle.net/1942/24946

Aqueous solution-gel precursors for $LiFePO_4$ lithium ion battery cathodes, their decomposition and phase formation

T. Vranken[a], W. Van Gompel[a], J. D'Haen[b], M. K. Van Bael[a] and A. Hardy[a]

a. *Inorganic and Physical Chemistry, Institute for Materials Research (IMO), UHasselt, Hasselt University, imec division imomec, Agoralaan building D, 3590 Diepenbeek, Belgium.*

b. Materials Physics, Institute for Materials Research (IMO), UHasselt, Hasselt University, imec division imomec, Wetenschapspark 1, 3590 Diepenbeek, Belgium.

Corresponding Author:

A. Hardy,

e-mail: an.hardy@uhasselt.be

tel: +3211268308

Several aqueous solution-gel precursors for the Li ion battery cathode material $LiFePO_4$, were synthesized. These differ in their composition, both regarding their Fe source, as well as in the complexing agent present. Fe(II) lactate hydrate is for the first time used as Fe^{2+} source. The ability to use an Fe^{3+} source (Fe(III) nitrate nonahydrate) for the synthesis of $LiFePO_4$ is also investigated. Our results show that it is possible to reduce the Fe^{3+} to Fe^{2+}, necessary to enable $LiFePO_4$ phase formation, during annealing under specific conditions. The decomposition behavior for these precursors in dry air, as well as in an inert atmosphere, is shown. Raman spectroscopy is used to evaluate the structure of the carbon phases present after annealing of the precursor powders.

$LiFePO_4$, Li ion battery, Cathode, Aqueous solution-gel synthesis, Iron lactate, Iron nitrate

Introduction

$LiFePO_4$ (LFP) is a member of the class of phospho-olivine cathode materials ($LiMPO_4$, with M = Fe, Mn, Ni, Co) for lithium ion batteries (LIB), which was discovered in 1997 [1, 2]. An important benefit of LFP in comparison with the original cathode in LIB, $LiCoO_2$ (LCO), is the fact that iron is much more abundant and thus significantly cheaper than cobalt. Iron is the fourth most abundant element in the earth's crust at 4.32%, while cobalt has an abundance of only 24 ppm [3]. On top of that, iron is also non-toxic. LFP has a theoretical capacity of 170 mAh g^{-1}, and a practical capacity nearing this value (up till around 160 mAh g^{-1}) [4]. While the theoretical capacity of LCO is significantly higher (274 mAh g^{-1}), its practical capacity is limited to only about 140 mAh g^{-1}, which corresponds with (de)intercalation in the range $0.5<x<1$ in Li_xCoO_2 [5]. The strong P-O covalent bonds in LFP increase the potential of the Fe^{3+}/Fe^{2+} redox couple, in comparison with its presence in an oxide lattice, to a value of 3.45 V, resulting in an improved competiveness compared to LCO (4.2 V) [4].

Disadvantages associated with phospho-olivine cathode materials are their low electronic conductivity ($< 10^{-9}$ S cm^{-1} for LFP) and low Li^+ diffusion coefficient ($\approx 10^{-14}$ cm^2 s^{-1} for LFP) [4, 6, 7]. The latter is a consequence of the crystal structure, in which Li^+ diffusion is only possible via narrow tunnels along the [010] crystallographic direction [8, 9]. The limited electrical conductivity and Li^+ diffusion coefficient come to expression at elevated (dis)charging rates. To reduce the effect of this intrinsically limited diffusion coefficient and conductivity, one generally reduces particle sizes and coats the particles with conductive carbon respectively [10].

In this article, we present several aqueous solution-gel based precursors for LFP. Upon annealing of the dried precursor powders in an inert argon atmosphere, a conductive carbon coating around the particles will be created by the decomposition of the complexing agents present. LFP has been reported to start crystallizing at around 450°C [11, 12]. An annealing temperature of at least 500°C is however necessary for the carbon phase to become conductive [13]. At temperatures higher than 750°C, an Fe_2P impurity phase is observed [13], which becomes dominant at

a temperature of 840°C [14]. Therefore, an annealing temperature of 650°C is used in this study.

Several precursors will be presented, differing mainly in their source of Fe ions and complexing agents. In $LiFePO_4$, the iron ion is present as Fe^{2+}. Therefore, an Fe(II) salt is preferred as a starting product. The anion of this salt should however not interfere with the chemistry of the other species in the precursor. Only a limited number of such salts are commercially available. We therefore investigated Fe(II) lactate hydrate as a novel inexpensive iron source in an aqueous solution-gel synthesis of LFP. Furthermore, we also investigated the compatibility of Fe(III) compounds with this synthesis route, by using Fe(III) nitrate nonahydrate, which is an inexpensively available Fe(III) source. Fe(III) nitrate nonahydrate was already used by Chen et al. [15], but resulted in that case in a $LiFePO_4(C+Fe_2P)$ composite. Lin et al. [16] also used Fe(III) nitrate nonahydrate for the synthesis of $LiFePO_4$. They however used a two-step heat treatment, ending with an anneal at 800°C in an Ar/H_2 95/5 atmosphere, using the H_2 present to reduce Fe(III). Another approach is to use a $FePO_4$ precursor, synthesized beforehand from Fe(III) nitrate nonahydrate, and combine this in an extra thermal step with Li_2CO_3 and an organic component in an inert [17] or reducing atmosphere [18, 19], to produce $LiFePO_4$. In our study, we show that by adjusting our synthesis conditions appropriately, Fe(III) from our dried precursor gels can be reduced and incorporated into the LFP lattice as Fe(II) during anneal without the use of any additional reactants, without the use of $FePO_4$ as an intermediary precursor, and without the use of H_2 as a reducing agent.

Experimental

Precursor synthesis

Aqueous precursor solutions for $LiFePO_4$ were prepared using an Fe-containing salt, LiH_2PO_4 (as source for Li^+ and PO_4^{3-}), and a complexing agent. Fe-containing salts studied were: Fe(II) lactate hydrate (≥ 98.0%, Sigma-Aldrich) and Fe(III) nitrate nonahydrate (ACS, ≥ 98%, Sigma-Aldrich). The hydrate content of the Fe(II) lactate hydrate starting product was quantified to be 2.1 H_2O molecules per formula unit by thermogravimetric analysis (TGA) and verified using inductively

coupled plasma optical emission spectroscopy (ICP-OES) before precursor synthesis. Complexing agents used were citric acid (CA) (99%, Sigma-Aldrich), ethylenediaminetetraacetic acid (EDTA) (Triplex® II, Merck) and L-ascorbic acid (AA) (≥ 98%, Sigma-Aldrich). Starting products were combined for the different precursors as listed in Table 1, were dissolved together in 70% of the final volume Milli-Q water and stirred under refluxing conditions at 50°C for 2 hours to obtain a clear solution. In the case of $Fe(NO_3)_3$ as iron source, it proved necessary to add the CA while stirring to a solution already containing the $Fe(NO_3)_3$ and LiH_2PO_4. In case of EDTA as the complexing agent, the dispersion remained turbid, and addition of ammonia (NH_3) (32 wt%, extra pure, Merck) after this heating step to the warm solution was necessary to fully dissolve the complexing agent to obtain a clear solution, hereby increasing the pH from ~2.3 to ~5.4. After cooling down the precursor solutions to room temperature, Milli-Q water was added to further dilute the precursors to the final concentrations. Solid precursor powders were obtained by drying the precursor solutions overnight at 80°C in a Binder lab oven, inducing gelation, and grinding them afterwards with a mortar and pestle.

Table 1: Precursor compositions.

Precursor	**LFP-1**	**LFP-2**	**LFP-3**	**LFP-4**
Li^+ and PO_4^{3-} source	LiH_2PO_4 (1 eq.)	LiH_2PO_4 (1 eq.)	LiH_2PO_4 (1 eq.)	LiH_2PO_4 (1 eq.)
Fe source	Fe(II) lactate hydrate (1 eq.)	Fe(II) lactate hydrate (1 eq.)	$Fe(III)(NO_3)_3$ (1 eq.)	$Fe(III)(NO_3)_3$ (1 eq.)
Complexing agent	CA (1 eq.)	EDTA (2 eq.)	CA (1 eq.)	AA (4 eq.)
NH_3 added?	No	Yes	No	No
Final concentration[1]	0.075 M	0.3 M	0.1 M	0.05 M

[1] With respect to "$LiFePO_4$ in solution".

Annealing

The precursor powders were annealed in an alumina crucible in a tube furnace. Unless mentioned otherwise, the standard program, consisting of a heating step to 650°C at 10°C/min, followed by an isothermal period of 4 hours in an argon atmosphere (0.5 L/min) (Alphagaz 1, 99.999%, Air Liquide), was used. Before starting the heating procedure, the tube containing the sample was flushed with Argon gas for 1 hour, to remove the oxygen.

Apparatus

ICP-OES analysis was done on a Perkin Elmer Optima 3000 DV. TGA was performed on a Dupont 951 Thermo Gravimetric Analyzer (standard procedure: 10°C/min to 700°C, 100 ml/min dry air atmosphere or He atmosphere). In the case of an experiment in He atmosphere, the TGA chamber was flushed for 1 hour with helium prior to each experiment to ensure an oxygen free environment during the heating. Powder X-ray diffraction (XRD) patterns were obtained on a Siemens Diffractometer D5000 (Cu $K_{\alpha 1}$ radiation). Raman spectra were recorded with a Horiba Jobin-Yvon T64000 spectrometer equipped with a confocal microscope. Excitation of the samples was performed with an Ar-ion 488 nm laser (Nexel 95). The instrument was calibrated using the Si (520.7 cm^{-1}) mode.

Results and discussion

Precursor decomposition behavior

Precursors based on Fe(II) lactate hydrate were prepared as described in the experimental section with CA (LFP-1) and EDTA (LFP-2) respectively, as well as a precursor based on Fe(III) nitrate nonahydrate with CA as complexing agent (LFP-3). The decomposition behavior of the dried and grinded precursor powders was studied using TGA. Decomposition behavior in dry air atmosphere was studied to learn about the thermo-oxidative decomposition behavior of the different precursors when oxygen is present. Results of this are shown in Figure 1. The lactate and CA containing precursor (LFP-1) is already almost completely decomposed (~60% mass loss) after a sudden mass loss around 232°C, while complete decomposition is obtained at around 400°C, making it the precursor with the lowest decomposition temperature. As pure CA shows a maximum decomposition rate at

~198°C when heated at 10°C/min under dry air atmosphere, and a maximum rate of mass loss at ~172°C was observed for pure Fe(II) lactate 2.1 H_2O, it is reasonable to assume the mass losses at ~215°C and ~232°C in the case of LFP-1 are related to the decomposition of lactato-citrato complexes [20]. The first one is also present in the decomposition of LFP-2 (EDTA – lactate precursor), corroborating its link with the decomposition of lactate complexes. LFP-2 clearly shows the largest mass loss (only ~18% remains). This can be understood by the fact that this precursor contains the largest amount of organics (i.e. ~585 g/mol for 2 eq. of EDTA vs. ~192 g/mol for 1 eq. of CA in LFP-1). The nitrate and CA containing LFP-3 precursor has the highest relative end mass, because of its limited presence of organics. The weight loss in the region between 130°C and 190°C is expected to be mainly related to the decomposition of nitrate [21]. The decomposition step with a maximum rate of mass loss at ~229°C can again be linked to the decomposition of CA.

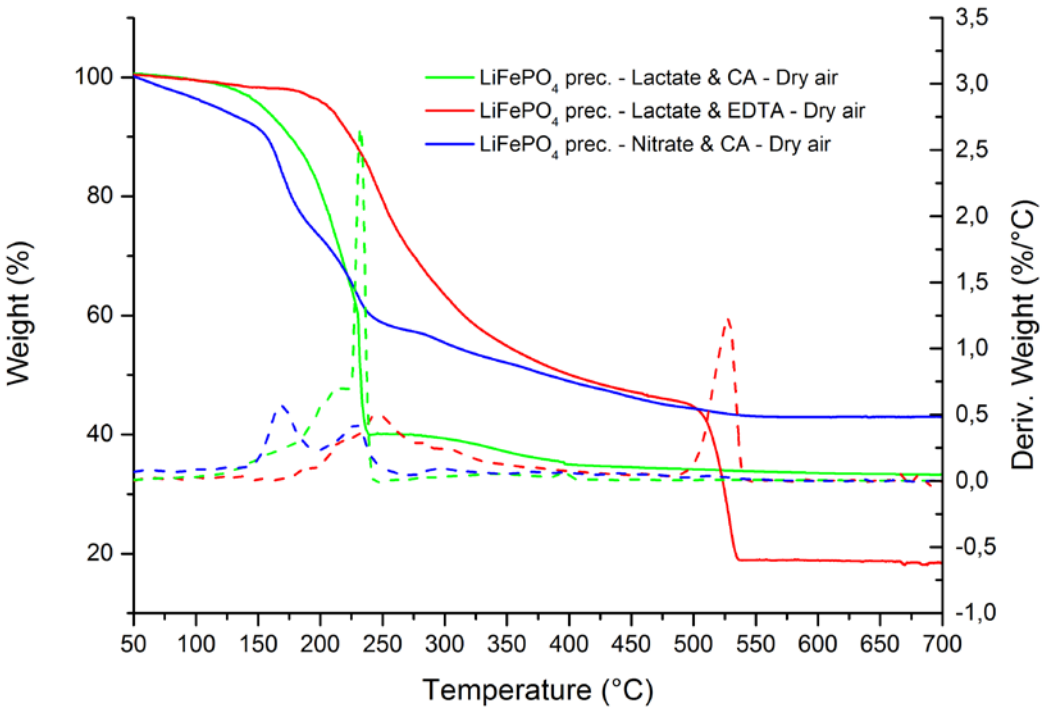

Figure 1: TGA of dry LFP precursor powders (green: LFP-1, red: LFP-2, blue: LFP-3). Heated at 10°C/min in dry air atmosphere.

Figure 2 shows the decomposition behavior of these precursors in an inert atmosphere (He). These decomposition experiments mimic the behavior during the actual annealing in a tube furnace in an inert argon atmosphere. Due to the lack of

oxygen present, oxidative decomposition is suppressed, resulting in a more gradual decomposition. The organic complexing agents are however only partially decomposed at the final temperature, as the final masses are higher than in an oxidative atmosphere (47.7% for LFP-1, 36.3% for LFP-2 and 41.1% for LFP-3). The residual organic content was converted to conductive carbon [13].

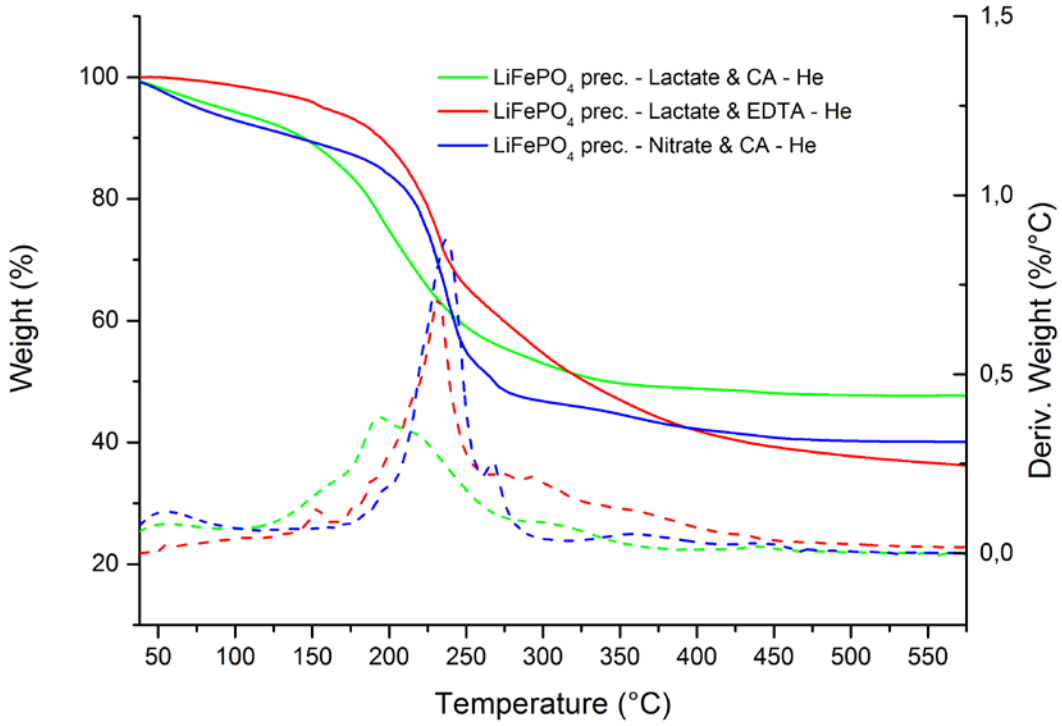

Figure 2: TGA of dry LFP precursor powders (green: LFP-1, red: LFP-2, blue: LFP-3). Heated at 10°C/min in helium atmosphere.

Phase formation

Annealing of the precursor powders was done at 650°C in argon atmosphere, as this is reported to be the optimum temperature for obtaining $LiFePO_4$ with a conductive carbon coating [13]. The product obtained after a standard anneal, as described in the experimental section, originating from a LFP-1 or LFP-2 precursor shows clearly the formation of the desired LFP phase in its powder X-ray diffractogram (LFP reference: ICDD card number 01-083-2092), as can be seen in Figure 3. No noticeable (crystalline) impurity phases are observed.

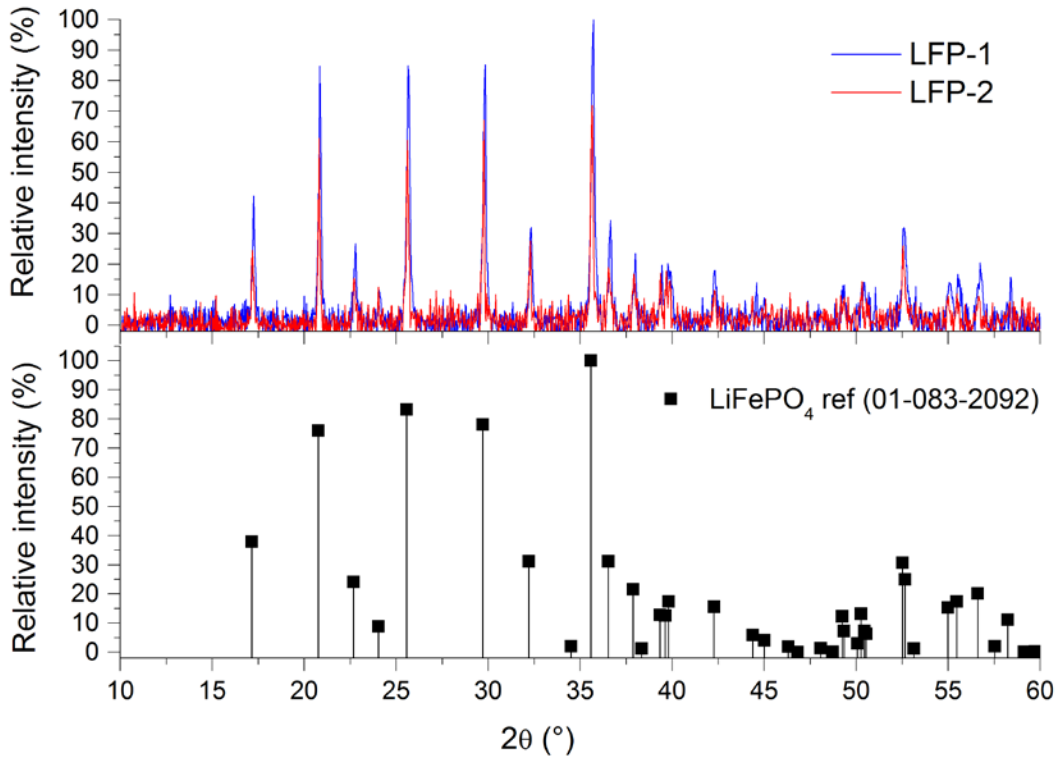

Figure 3: XRD patterns of precursors LFP-1 (lactate – CA precursor) in blue and LFP-2 (lactate – EDTA precursor) in red after annealing, together with the LFP reference pattern (ICDD 01-083-2092).

Diffraction peaks corresponding to LFP could however not be observed in the XRD pattern of the annealed LFP-3 precursor, using the same annealing treatment as for LFP-1 and LFP-2. Instead of phase pure LFP, a mixture of several phases was formed. In this pattern, shown in Figure 4, peaks are assigned to Li_3PO_4, and phases containing Fe(III): β-Fe_2O_3 and Fe_3PO_7. These are reported as common impurities in the synthesis of LFP [13, 22, 23]. It is clear that the processing parameters during the anneal did not allow the Fe^{3+} ions, originating from Fe(III) nitrate to be reduced to Fe^{2+}. We conclude that this is necessary to be able to form the $LiFePO_4$ phase.

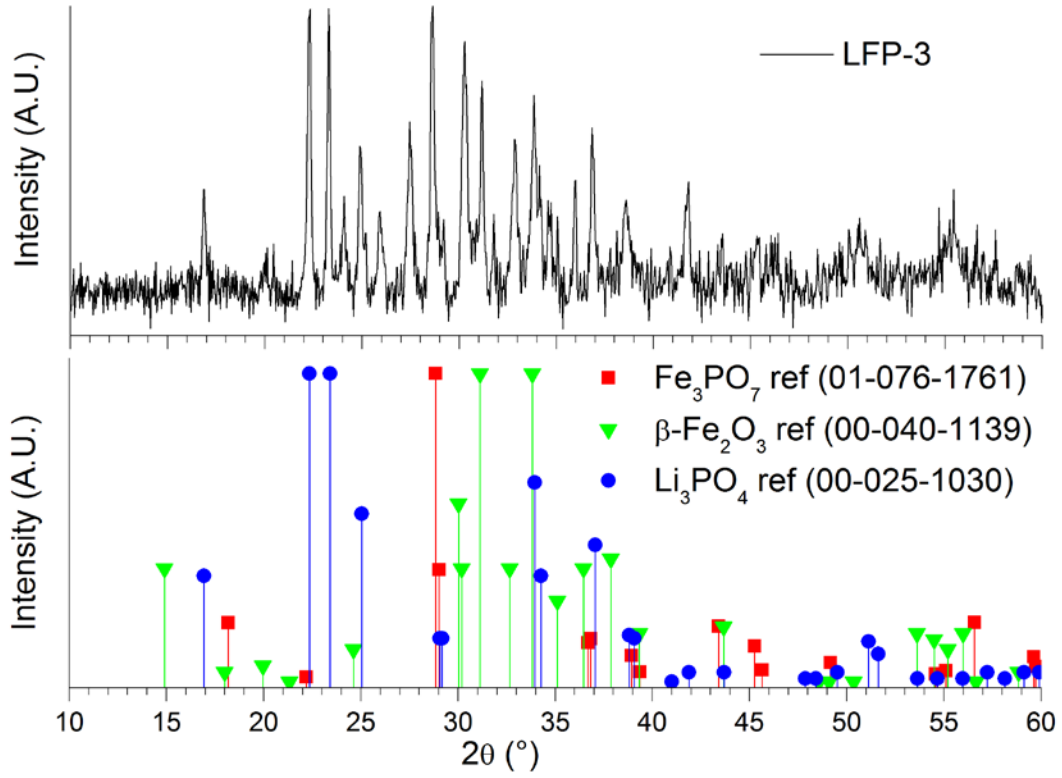

Figure 4:XRD pattern of a LFP-3 (Fe(III) nitrate – CA) precursor powder after a standard annealing procedure together with ICDD references patterns of Fe_3PO_7, β-Fe_2O_3 and Li_3PO_4.

Subsequently, the parameters of the standard annealing process were varied, studying if these new conditions would enable the reduction of Fe^{3+} ions from the LFP-3 precursor to Fe^{2+} during the anneal. One approach encompassed a decrease of the heating rate. Decreasing this rate from the standard 10°C/min to 2°C/min did indeed enable reduction of Fe^{3+}, as the XRD pattern of this product shows again a phase pure LFP product (as can be seen in Figure 5a). On the other hand, also a longer isothermal step in the annealing process was investigated. By heating the sample again at the standard rate of 10°C/min to 650°C, but keeping the sample in the flowing argon atmosphere for 24h instead of 4h, the Fe^{3+} could again be reduced to Fe^{2+}, resulting in a phase pure LFP product (shown in Figure 5b). Both results show that LFP can indeed be formed from a precursor containing Fe^{3+} and no organic material other than the 1 eq. of CA used as the complexing agent in the solution-gel synthesis. These results can be explained by taking a closer look at the processes occurring during the anneal in an inert atmosphere. It has been reported that reducing gases (hydrogen and hydrocarbon gasses) are produced during the pyrolysis of the organic material present in the precursor powders. These reducing gasses allow the formation of conductive carbon out of partly decomposed organics,

as well as enable the reduction of Fe^{3+} [13, 24–27]. A slower heating rate, results in a more gradual decomposition of the organics and more gradual evolution of reducing gasses. Our results show that this enhances the reduction of Fe^{3+}. The longer annealing period also enables the reduction of Fe^{3+}. This might be explained by carbothermal reduction, where the conductive carbon formed throughout the sample, allows the reduction of Fe^{3+}. Although according to Ravet et al. [26], the process of Fe^{3+} reduction by carbon is only efficient at temperatures starting around about 1000°C, the long annealing time of 24h might still allow this reduction, possibly catalyzed by the presence of the (precursors of) $LiFePO_4$.

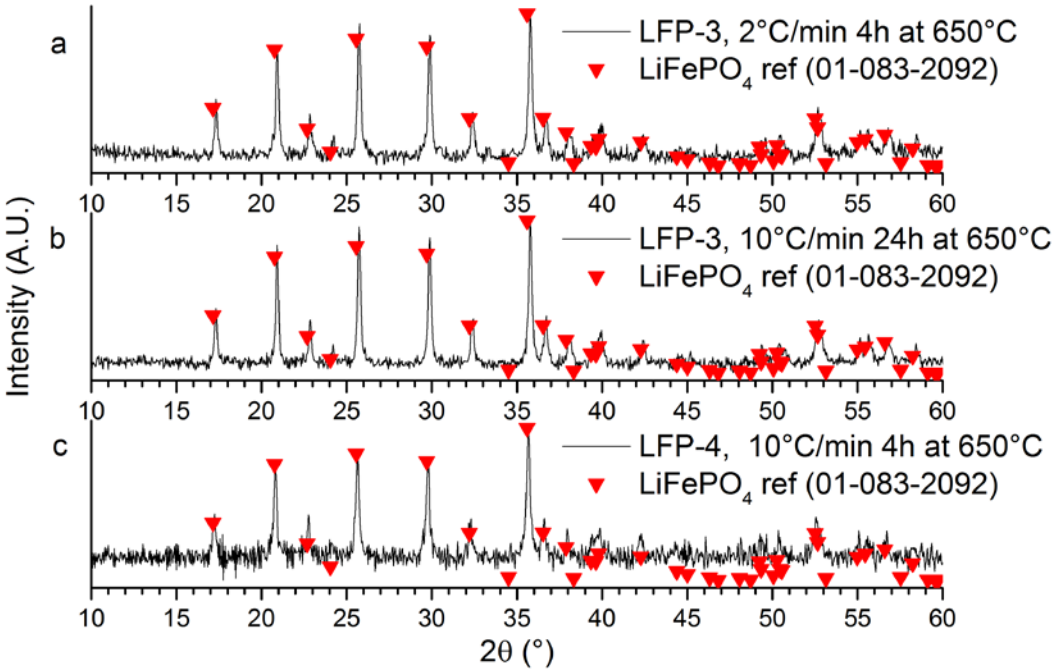

Figure 5: X-ray diffractograms of (a) LFP-3 precursor, annealed at a heating rate of 2°C/min instead of 10°C/min, (b) annealed for 24h instead of 4h, and (c) LFP-4 precursor, in which 1 eq. of CA was changed for 4 eq. of AA. All these modifications allowed the reduction of Fe^{3+} to Fe^{2+} and subsequently LFP phase formation.

Instead of modifying the annealing process (heating rate and isothermal period) to reduce the Fe^{3+}, it was also found that modifying the precursor composition can also enable the formation of LFP using the standard annealing process parameters. This new precursor (LFP-4) differs from the LFP-3 precursor composition by replacing the 1 eq. of CA by 4 eq. of ascorbic acid, as ascorbic acid is known for its ability to reduce Fe(III) to Fe(II) in solution [28]. This hypothesis was also verified by adding a small amount of a solution of KSCN to the precursor solution. In the

presence of free Fe^{3+} species, this would result in a deep-red color change, due to the formation of $Fe(III)(SCN)_3$ complexes. This was however not observed, indicating that the Fe^{3+} was indeed already completely reduced to Fe^{2+} in solution. It is, however, known that this qualitative analysis may suffer from interference in the presence of phosphate ions, as these can form stable Fe^{3+} complexes [29]. In order to exclude this interference, new solutions were prepared, which did not contain LiH_2PO_4. Also in this case, no deep-red color change was observed, indicating that the Fe^{3+} is truly reduced to Fe^{2+} in solution in the presence of ascorbic acid. We furthermore observed that this reduction reaction happens instantaneously upon mixing $Fe(III)(NO_3)_3$ and ascorbic acid in water, even without any heating. The photograph in Figure 6 includes samples of $Fe(III)(NO_3)_3$ and ascorbic acid before and after addition of KSCN (c and d respectively), while also showing $Fe(III)(NO_3)_3$ without and with KSCN added (a and b respectively), the latter showing the typical deep-red color of $Fe(III)(SCN)_3$ as a reference. The phase pure result after a standard anneal using the LFP-4 precursor can be seen in Figure 5c.

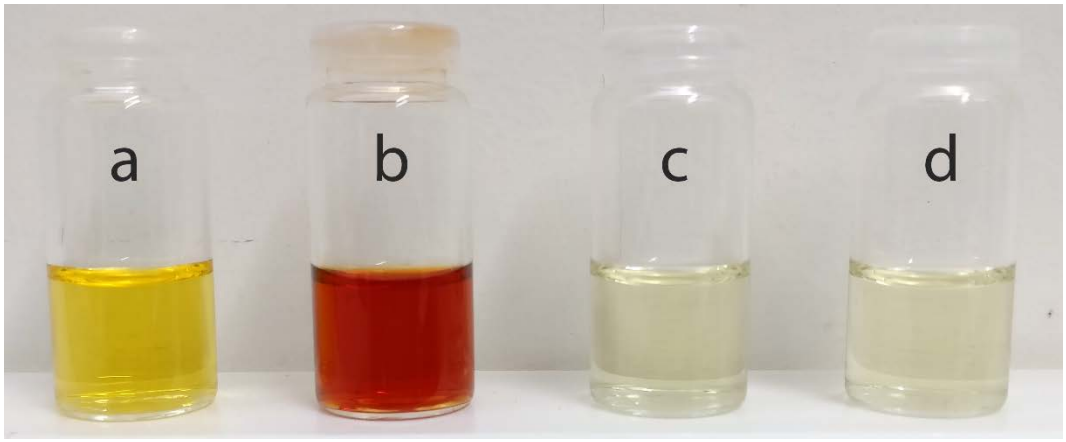

Figure 6: Photograph showing from left to right solutions of: (a) $Fe(III)(NO_3)_3$, (b) $Fe(III)(NO_3)_3$ + KSCN, (c) $Fe(III)(NO_3)_3$ + ascorbic acid, (d) $Fe(III)(NO_3)_3$ + ascorbic acid + KSCN. Sample (b) shows the typical deep-red color of the $Fe(III)(SCN)_3$ complex, which forms in the presence of free Fe^{3+}. In sample (d), which in addition also contains ascorbic acid, no such color is observed, indicating that the Fe^{3+} is already reduced to Fe^{2+}.

Conductive carbon

Raman spectroscopy was used to get an understanding of the structure of the carbon present in the LFP samples after anneal. This (conductive) carbon present at the particle surfaces enhances the electronic conductivity of the LFP particles, which is

an important parameter for its application in LIB cathodes. Figure 7 shows the Raman spectra for different product powders in the region between 1000 cm^{-1} and 2000 cm^{-1}. The broad bands centered on ~1350 cm^{-1} and ~1600 cm^{-1} correspond to what are commonly called the D- (disordered) and G- (graphite) bands of carbon respectively. These bands are however both composed of two major peaks, with their relative contribution depending on the carbon structure [13]. In order to semi-quantitatively assess the shape of these bands, deconvolution is necessary. Deconvolution procedures for carbon D- and G-bands have been described before in literature [27, 30–33]. Our deconvolution procedure was based on Maccario et al. [33], fitting the 4 peaks with a Voigt peak profile as in Golabczak et al. [34]. Fitting results are shown in Table 2. $R^2 > 0.98$ was obtained for all fits. The peaks at ~1200 cm^{-1} and ~1530 cm^{-1} which are situated next to the actual D- and G- peaks in the D- and G-bands respectively, are commonly assigned to vibrations related to sp^3-type carbon [27, 31, 35]. The actual D-peak is situated at ~1350-1360 cm^{-1} [27, 30, 33]. In a perfectly ordered graphene sheet [36], it would not occur, as it is a disorder-allowed mode [37, 38]. The peak with a maximum at ~1600 cm^{-1} is the actual G-peak, which is linked to the in-plane vibrational mode of the movement of two carbon atoms moving in opposite directions in a graphene sheet [36]. A parameter that has been used to relate the Raman spectrum of a carbon coating to its electronic conductivity is the relative (integrated) intensity ratio of the D- and G-peaks: $R = I_D/I_G$ [39]. A lower value for this ratio corresponds to a less disordered carbon phase, resulting in a higher expected conductivity. As can be seen in the fitting data, shown in Table 2, $R = I_D/I_G$ is calculated to be 1.86, 1.57 and 2.02 for annealed products originating from LFP-1, LFP-2 and for LFP-3 respectively. Although the differences in R are not that pronounced, the annealed product resulting from LFP-2 is expected to be slightly superior in terms of electronic conductivity. Since the structure of the carbon present after annealing is reported to be dependent on the nature of the organic material present in the precursor powder [40], these results are reasonable.

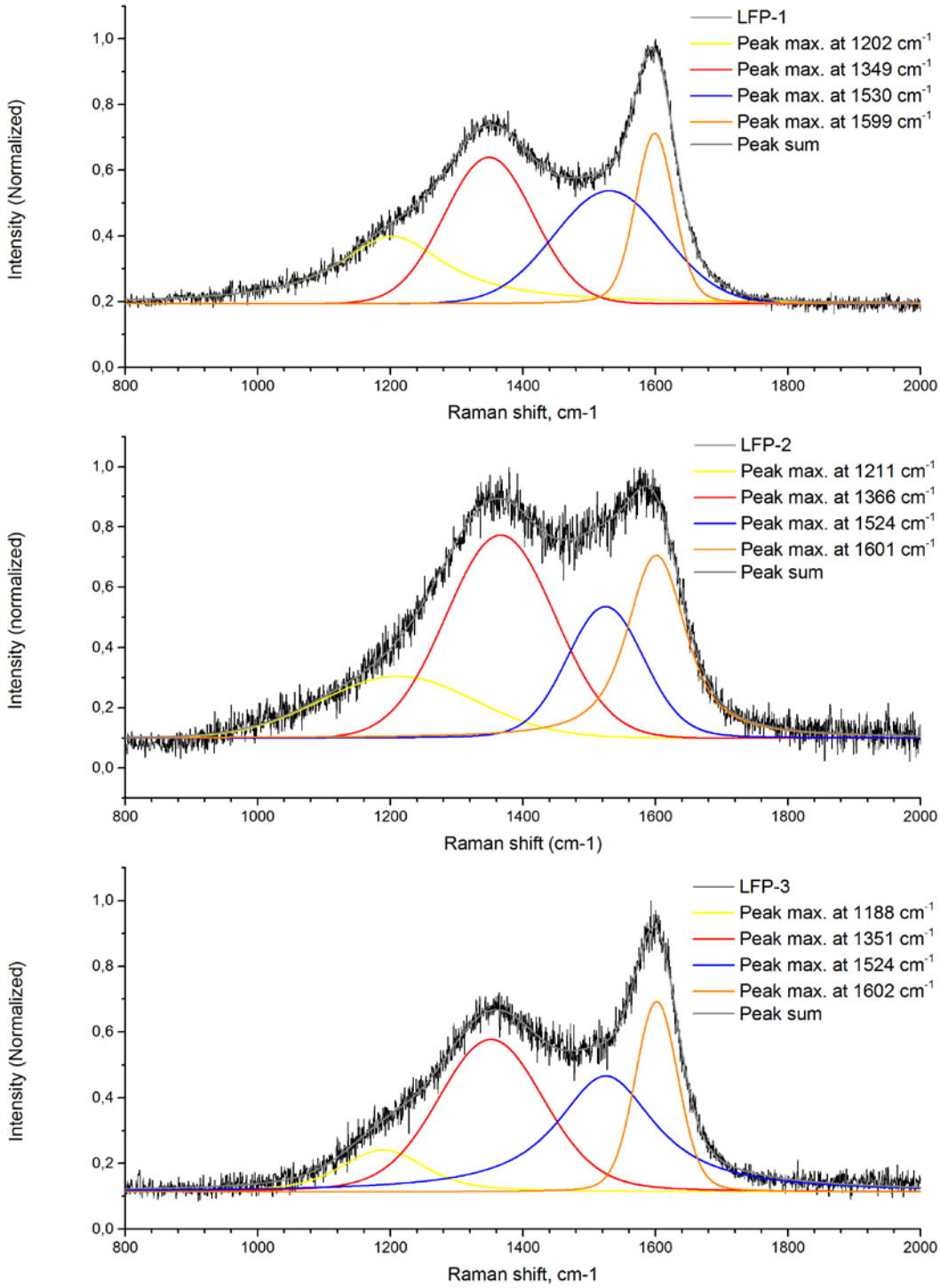

Figure 7: Deconvoluted Raman spectra of LFP-1, LFP-2 and LFP-3 annealed powders.

Table 2: Parameters of the fitted Voigt peaks in the Raman spectra of LFP-1, LFP-2 and LFP-3.

LFP-1	LFP-2	LFP-3
Peak positions (cm^{-1})		
1202	1211	1188
1349 (D)	1366 (D)	1352 (D)
1530	1525	1525
1599 (G)	1601 (G)	1602 (G)
Peak areas (arbitrary units)		
63.81	60.12	25.27
75.35 (D)	138.33 (D)	101.13 (D)
72.05	66.95	97.93
40.54 (G)	88.12 (G)	50.02 (G)
Voigt FWHM (cm^{-1})		
198.30	275.40	151.33
158.86 (D)	192.95 (D)	189.17 (D)
196.92	137.45	179.32
68.44 (G)	104.19 (G)	76.06 (G)
I_D/I_G		
1.86	1.57	2.02

Conclusions

We showed that $LiFePO_4$ can be synthesized via an aqueous solution-gel method, both when the precursor contains an Fe(II) salt, as well as when it contains an Fe(III) salt. As the iron ion is in the 2+ state in $LiFePO_4$, a reduction to Fe(II) is necessary during synthesis when using a Fe(III) salt. This reduction can be enabled due to the reducing gasses, produced by the decomposition of organic complexing agents present in the precursor, in an inert atmosphere during annealing. However, we showed that this reduction only happens optimally under specific process conditions. The heating rate is an important controlling parameter, as a slower heating rate will ensure a longer contact time of the sample with the reducing decomposition gasses. Increasing annealing time also improved the reduction reaction. Apart from a longer contact time with reducing gasses, carbothermal reduction of the sample with the formed carbon phase can also enhance reduction.

Raman spectroscopy indicates the presence of conducting carbon in all annealed samples. We have shown that the choice of the organic complexing agents influences the structure of the conductive carbon, which will ultimately influence battery performance (especially rate performance). The ratio $R = I_D/I_G$ is the smallest for the Fe(II) lactate – EDTA based precursor, indicative for the best conductive carbon present.

Acknowledgements

The authors would like to acknowledge Ken Elen for carrying out the XRD measurements and Dries De Sloovere for TGA measurements. Thomas Vranken is a Ph.D. fellow of the Research Foundation – Flanders (FWO). The authors declare no competing financial interest.

References

1. Padhi AK, Nanjundaswamy KS, Goodenough JB (1997) Phospho-olivines as positive-electrode materials for rechargeable lithium batteries. J Electrochem Soc 144:1188–1194. doi: 10.1149/1.1837571
2. Yamada A, Chung S-C (2001) Crystal Chemistry of the Olivine-Type Li(Mn[sub y]Fe[sub 1−y])PO[sub 4] and (Mn[sub y]Fe[sub 1−y])PO[sub 4] as Possible 4 V Cathode Materials for Lithium Batteries. J Electrochem Soc 148:A960. doi: 10.1149/1.1385377
3. Wedepohl KH (1995) The composition of the continental crust. Geochim Cosmochim Acta 59:1217–1232. doi: 10.1016/0016-7037(95)00038-2
4. Julien CM, Mauger A, Zaghib K, Groult H (2014) Comparative Issues of Cathode Materials for Li-Ion Batteries. Inorganics 2:132–154. doi: 10.3390/inorganics2020132
5. Nazri G-A, Pistoia G (2004) Lithium Batteries: Science and Technology. Lithium Batter Sci Technol. doi: 10.1007/978-0-387-92675-9
6. Sauvage F, Baudrin E, Gengembre L, Tarascon J-M (2005) Effect of texture on the electrochemical properties of LiFePO4 thin films. Solid State Ionics 176:1869–1876. doi: 10.1016/j.ssi.2005.05.012
7. Delacourt C, Poizot P, Morcrette M, et al (2004) One-Step Low-Temperature Route for the Preparation of Electrochemically Active LiMnPO4 Powders. Chem Mater 16:93–99. doi: 10.1021/cm030347b

8. Nishimura S, Kobayashi G, Ohoyama K, et al (2008) Experimental visualization of lithium diffusion in LixFePO4. Nat Mater 7:707–711. doi: 10.1038/nmat2251
9. Islam MS, Driscoll DJ, Fisher CAJ, Slater PR (2005) Atomic-Scale Investigation of Defects , Dopants , and Lithium Transport in the LiFePO4 Olivine-Type Battery Material. Chem Mater 17:5085–5092. doi: 10.1021/cm050999v
10. Park OK, Cho Y, Lee S, et al (2011) Who will drive electric vehicles, olivine or spinel? Energy Environ Sci 4:1621. doi: 10.1039/c0ee00559b
11. Hasegawa G, Ishihara Y, Kanamori K, et al (2011) Facile preparation of monolithic LiFePO4/carbon composites with well-defined macropores for a lithium-ion battery. Chem Mater 23:5208–5216. doi: 10.1021/cm2021438
12. Gaberscek M, Dominko R, Bele M, et al (2006) Mass and charge transport in hierarchically organized storage materials. Example: Porous active materials with nanocoated walls of pores. Solid State Ionics 177:3015–3022. doi: 10.1016/j.ssi.2006.07.060
13. Zaghib K, Mauger A, Julien CM (2012) Overview of olivines in lithium batteries for green transportation and energy storage. J Solid State Electrochem 16:835–845. doi: 10.1007/s10008-011-1629-8
14. Toprakci O, Toprakci H a K, Ji L, Zhang X (2010) Fabrication and Electrochemical Characteristics of LiFePO 4 Powders for Lithium-Ion Batteries. KONA Powder Part J 28:50–73. doi: 10.14356/kona.2010008
15. Chen Q, Li X, Wang J (2011) Electrochemical performance of LiFePO4/(C+Fe2P) composite cathode material synthesized by sol-gel method. J Cent South Univ Technol 18:978–984. doi: 10.1007/s11771-011-0790-7
16. Lin H, Yeh S, Chen J (2014) Physical and Electrochemical Properties of LiFePO 4 / C Nanofibers Synthesized by Electrospinning. Int J Electrochem Sci 9:6936–6948.
17. Yang G, Jiang CY, He XM, et al (2013) Preparation of Li3V2 (PO4)3/LiFePO4 composite cathode material for lithium ion batteries. Ionics (Kiel) 19:1247–1253. doi: 10.1007/s11581-013-0856-7
18. Xie H-M, Wang R-S, Ying J-R, et al (2006) Optimized LiFePO4–Polyacene Cathode Material for Lithium-Ion Batteries. Adv Mater 18:2609–2613. doi:

10.1002/adma.200600578

19. Oh SW, Myung ST, Oh SM, et al (2010) Double carbon coating of LiFePO4 as high rate electrode for rechargeable lithium batteries. Adv Mater 22:4842–4845. doi: 10.1002/adma.200904027
20. Barbooti MM, Al-Sammerrai DA (1986) Thermal decomposition of citric acid. Thermochim Acta 98:119–126. doi: 10.1016/0040-6031(86)87081-2
21. Wieczorek-Ciurowa K, Kozak AJ (1999) The thermal decomposition of Fe(NO3)3×9H2O. J Therm Anal Calorim 58:647–651. doi: 10.1063/1.3253104
22. Yu DYW, Donoue K, Kadohata T, et al (2008) Impurities in LiFePO(4) and their influence on material characteristics. J Electrochem Soc 155:A526–A530. doi: 10.1149/1.2919105
23. Zhou N, Wang HY, Uchaker E, et al (2013) Additive-free solvothermal synthesis and Li-ion intercalation properties of dumbbell-shaped LiFePO4/C mesocrystals. J Power Sources 239:103–110. doi: 10.1016/j.jpowsour.2013.03.136
24. Chen Z, Qin Y, Amine K, Sun Y-K (2010) Role of surface coating on cathode materials for lithium-ion batteries. J Mater Chem 20:7606. doi: 10.1039/c0jm00154f
25. Kim K, Cho Y-H, Kam D, et al (2010) Effects of organic acids as reducing agents in the synthesis of LiFePO4. J Alloys Compd 504:166–170. doi: 10.1016/j.jallcom.2010.05.078
26. Ravet N, Gauthier M, Zaghib K, et al (2007) Mechanism of the Fe3+ reduction at low temperature for LiFePO4 synthesis from a polymeric additive. Chem Mater 19:2595–2602. doi: 10.1021/cm070485r
27. Zhao RR, Ma GZ, Zhu LC, et al (2012) An improved Carbon-Coating Method for LiFePO 4 / C composite derived from Fe 3 + precursor. Int J Electrochem Sci 7:10923–10932.
28. Elmagirbi A, Sulistyarti H, Atikah (2012) Study of Ascorbic Acid as Iron(III) Reducing Agent for Spectrophotometric Iron Speciation. J Pure Appl Chem Res 1:11–17.
29. Vogel A, Svehla G (1979) Vogel's Textbook of Macro And Semimicro Qualitative Inorganic Analysis, 5th ed. Longman, London
30. Kumar A, Thomas R, Karan NK, et al (2009) Structural and Electrochemical

Characterization of Pure LiFePO4 and Nanocomposite C-LiFePO4 Cathodes for Lithium Ion Rechargeable Batteries. J Nanotechnol 2009:1–10. doi: 10.1155/2009/176517

31. Fey GT-K, Tu H-J, Huang K-P, et al (2012) Particle size effects of carbon sources on electrochemical properties of LiFePO4/C composites. J Solid State Electrochem 16:1857–1862. doi: 10.1007/s10008-011-1621-3
32. Kostecki R, Schnyder B, Alliata D, et al (2001) Surface studies of carbon films from pyrolyzed photoresist. Thin Solid Films 396:36–43. doi: 10.1016/S0040-6090(01)01185-3
33. Maccario M, Croguennec L, Desbat B, et al (2008) Raman and FTIR Spectroscopy Investigations of Carbon-Coated Li[sub x]FePO[sub 4] Materials. J Electrochem Soc 155:A879. doi: 10.1149/1.2977961
34. Gołąbczak M, Konstantynowicz a (2009) Raman spectra evaluation of the carbon layers with Voigt profile. J Achiev Mater Manuf Eng 37:270–276.
35. Doeff MM, Wilcox JD, Yu R, et al (2008) Impact of carbon structure and morphology on the electrochemical performance of LiFePO4/C composites. J Solid State Electrochem 12:995–1001. doi: 10.1007/s10008-007-0419-9
36. Hsu K-F, Tsay S-Y, Hwang B-J (2004) Synthesis and characterization of nano-sized LiFePO4 cathode materials prepared by a citric acid-based sol?gel route. J Mater Chem 14:2690.
37. Hong J, Wang C, Dudney NJ, Lance MJ (2007) Characterization and Performance of LiFePO[sub 4] Thin-Film Cathodes Prepared with Radio-Frequency Magnetron-Sputter Deposition. J Electrochem Soc 154:A805. doi: 10.1149/1.2746804
38. Yan X, Yang G, Liu J, et al (2009) An effective and simple way to synthesize LiFePO4/C composite. Electrochim Acta 54:5770–5774. doi: 10.1016/j.electacta.2009.05.048
39. Julien CM, Zaghib K, Mauger A, et al (2006) Characterization of the carbon coating onto LiFePO4 particles used in lithium batteries. J Appl Phys. doi: 10.1063/1.2337556
40. Wang J, Sun X (2012) Understanding and recent development of carbon coating on LiFePO4 cathode materials for lithium-ion batteries. Energy Environ Sci 5:5163. doi: 10.1039/c1ee01263k